 MCB, vol.6, no.2, pp.93-99, 2009

The Mechanical Buckling of Curved Arteries*

Hai-Chao Han†

Abstract: Though tortuosity and kinking are often observed in various arteries and arterioles, little is known about the underlying mechanisms. This paper presents a biomechanical analysis of bent buckling in long arterial segments with a small initial curvature using a thick-walled elastic cylindrical arterial model. The critical buckling pressure was established as a function of wall stiffness, wall dimensions, and the axial tension (or axial stretch ratio). The effects of both wall dimensions and axial stretch ratio on the critical pressure, as well as the thin-walled approximation were discussed. The buckling equation sheds light on the biomechanical mechanism of artery tortuosity and provides guidance for the development of new techniques to treat and prevent artery tortuosity and kinking.

Keyword: artery buckling, tortuosity, stability, thick wall model, initial curvature

1 Introduction

Arterial tortuosity, often associated with aging, hypertension, and atherosclerosis, occurs in many patients with significant clinical complications (Metz et al. 1961; Weibel and Fields 1965; Weibel and Fields 1965; Del Corso et al. 1998; Pancera et al. 2000; Dawson et al. 2002; Thore et al. 2007). However, the underlying mechanism of arterial tortuosity remains poorly understood. Normal arteries *in vivo* are subjected to significant blood pressure and axial (longitudinal) tension (Han and Fung 1995; Nichols and O'Rourke 1998; Humphrey 2002). The axial tension and pressure in arteries may change due to aging or vascular disease. For example, while hypertension becomes prevalent with aging, axial tension decreases significantly with aging (Han and Fung 1995; Nichols and O'Rourke 1998; Humphrey 2002). We have shown recently that cylindrical arteries may buckle (bend) due to increased pressure or reduced axial stretch (Han 2007). In the long-term, loss of mechanical stability due to buckling may lead to arterial tortuosity. Our previous buckling equation was established for a linear elastic, thin-walled, straight cylindrical artery model; However, arteries are often nonlinear elastic and slightly curved. According to column buckling theory, this "imperfection" may affect the stability of the structure (Gere 2004). Therefore, the objective of this study was to establish the buckling equation for thick-walled, nonlinear elastic, and slightly curved arteries.

2 The Mechanical Model

The arteries are modeled as nonlinear elastic, thick-walled, circular cylinders with a small curvature. Let the lumen radius, wall thickness, and length of an artery under pressure p and axial tension N be designated as a, t, and L, respectively. The axial stress and stretch ratio in the artery are denoted by σ_z and λ_z, respectively. For simplicity, we assume the shape of the axial (longitudinal) axis is a half-sine wave and the artery has two open ends that are pin-supported (free to rotate but restricted from lateral movement). In the small pressure range, the artery is stable and deforms under pressure with its shape defined for each pressure load. The central axis of the artery under the pressure and axial tension is given by

$$x_c = C \cdot \sin\left(\frac{\pi z}{l}\right) \tag{1}$$

* Dedicate to Dr. Y. C. Fung

† Department of Mechanical Engineering, University of Texas at San Antonio, Biomedical Engineering Program, UTSA-UTHSCSA, San Antonio, TX 78249; Tel: (210) 458-4952; Fax: (210) 458-6504; E-mail: haichao.han@utsa.edu

where, C is a (small) constant and z is the coordinate in the axial direction (Fig. 1).

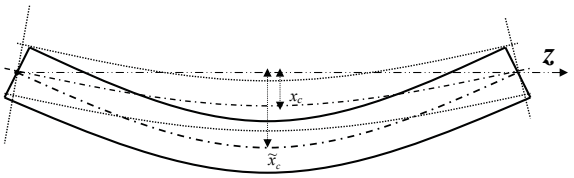

Figure 1: Schematic illustration of the shape of a curved arterial segment under internal pressure and axial stretch and the definition of the z axis. Dotted lines indicate the initial shape.

When the pressure reaches critical pressure, the artery will become unstable and can bend further without increasing pressure. Let's consider the beginning of the buckling process when the artery bends a small amount and the central axis deforms into a new half-sine wave shape:

$$\tilde{x}_c = \tilde{C} \cdot \sin\left(\frac{\pi z}{L}\right) \tag{2}$$

Where $\tilde{C}$ is a constant ($\tilde{C} > C$).

In both configurations, the lumen surface area is uneven on the concave and convex sides of the artery (Fig. 2). Thus, the internal pressure p generates an uneven lateral load that leads to a distributed lateral load $q(z)$ along the artery (Han 2007).

$$\begin{aligned} q(z) &= \int_0^{2\pi} p(ad\varphi)\left(\frac{\partial^2 x_c}{\partial z^2}\right)(a\cos\varphi)\cos\varphi \\ &= C\frac{p\pi^3 a^2}{l^2}\sin\left(\frac{\pi z}{l}\right) \\ \tilde{q}(z) &= \int_0^{2\pi} p(ad\varphi)\left(\frac{\partial^2 \tilde{x}_c}{\partial z^2}\right)(a\cos\varphi)\cos\varphi \\ &= \tilde{C}\frac{p\pi^3 a^2}{l^2}\sin\left(\frac{\pi z}{l}\right) \end{aligned} \tag{3}$$

The load $q(z)$is balanced by the axial tension N and lateral restriction forces Q at the ends (Fig. 2 bottom). Thus, the lateral reaction force Q and

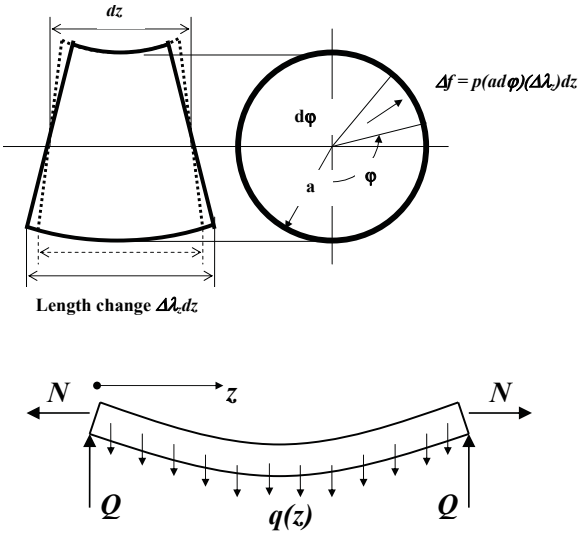

Figure 2: Top: Schematics of a small segment dz in a buckled artery illustrating the change in uneven surface area due to the deformation and the surface load generated by the internal pressure. Dotted lines indicate the initial shape. Bottom: A free-body diagram of a buckled artery with pinned ends. Q represents the lateral reactive force. N represents the axial tension, and $q(z)$ represents the pressure-generated distributed lateral load.

bending moment M at axial location z can be determined using the equations of equilibrium.

$$\begin{aligned} Q &= \frac{1}{2}\int_0^L q(z)dz = \frac{p\pi^2 a^2}{L}C \\ \tilde{Q} &= \frac{1}{2}\int_0^L \tilde{q}(z)dz = \frac{p\pi^2 a^2}{L}\tilde{C} \end{aligned} \tag{4}$$

and

$$\begin{aligned} M &= Q\cdot z - N\cdot C\cdot\sin\left(\frac{\pi z}{L}\right) - \int_0^z q(\xi)d\xi(z-\xi) \\ \tilde{M} &= \tilde{Q}\cdot z - \tilde{N}\cdot\tilde{C}\cdot\sin\left(\frac{\pi z}{L}\right) - \int_0^z \tilde{q}(\xi)d\xi(z-\xi) \end{aligned} \tag{5}$$

Therefore, the incremental bending increases the uneven surface area that generates an incremental

distributed lateral load $\Delta q(z)$ and an incremental bending moment:

$$\Delta M = (\Delta Q)z - (\tilde{N}\cdot\tilde{C} - N\cdot C)\cdot\sin\left(\frac{\pi z}{L}\right) - \int_0^z \Delta q(\xi)d\xi(z-\xi) \quad (6)$$

Taking equations (3)–(5) into (6) gives

$$\Delta M = (p\pi a^2)(\tilde{C}-C)\cdot\sin\left(\frac{\pi z}{L}\right) - (\tilde{N}\cdot\tilde{C} - N\cdot C)\cdot\sin\left(\frac{\pi z}{L}\right) \quad (7)$$

On the other hand, the axial tension N and bending moment M can be obtained by integrating the stress σ_z over the cross-sectional area A:

$$\begin{aligned} N &= \int_A \sigma_z dA, \quad M = \int_A (\sigma_z dA)(r\cos\varphi) \\ \tilde{N} &= \int_A \tilde{\sigma}_z dA, \quad \tilde{M} = \int_A (\tilde{\sigma}_z dA)(r\cos\varphi) \end{aligned} \quad (8)$$

Where r is the radial coordinate of points in the cross section, $r \in (a, a+t)$. Therefore,

$$\begin{aligned} \tilde{N} &= N + \int_A (\Delta\sigma_z)dA, \\ \Delta M &= \int_A (\Delta\sigma_z dA)(r\cos\varphi) \end{aligned} \quad (9)$$

where $\Delta\sigma_z$ is the incremental axial stress.

The increase of deflection from x_c to $\tilde{x}_c$ leads to incremental radial, circumferential, and axial displacements of point (r, φ, z), designated Δu, Δv and Δw, respectively (Figure 3):

$$\begin{aligned} \Delta u &= (\tilde{C}-C)\cos\varphi\sin\left(\frac{\pi z}{L}\right) \\ \Delta v &= -(\tilde{C}-C)\sin\varphi\sin\left(\frac{\pi z}{L}\right) \\ \Delta w &= -\frac{\pi_r}{L}(\tilde{C}-C)\cos\varphi\cos\left(\frac{\pi z}{L}\right) \end{aligned} \quad (10)$$

Thus, the incremental axial stretch ratio $\Delta\lambda_z$ caused by the incremental bending is

$$\Delta\lambda_z = \frac{\partial(\Delta w)}{\partial z} = \frac{\pi^2 r}{L^2}(\tilde{C}-C)\cos\varphi\sin\left(\frac{\pi z}{L}\right) \quad (11)$$

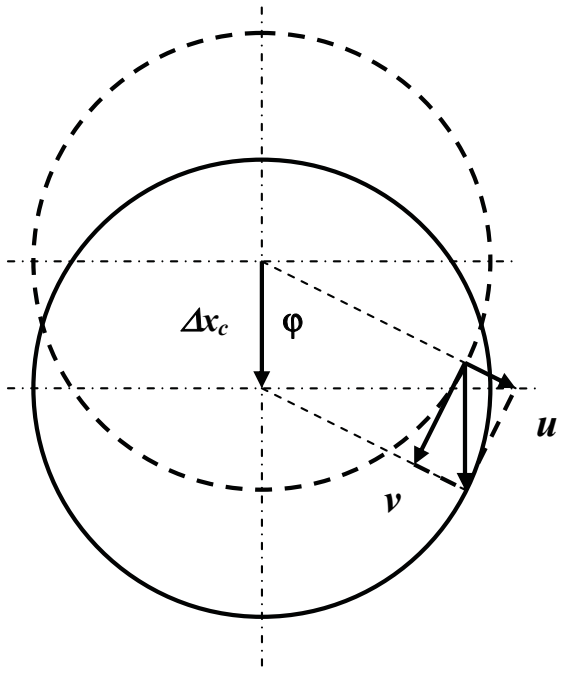

Figure 3: Schematic illustration of polar angle φ and the relationship between the incremental radial displacement u, circumferential displacement v and the incremental deflection Δx_c of the central axis. Dotted lines indicate the initial position.

The corresponding axial stress can be determined by

$$\Delta\sigma_z = E_t(\Delta\lambda_z) = \frac{E_t\pi^2 r}{L^2}(\tilde{C}-C)\cos\varphi\sin\left(\frac{\pi z}{L}\right) \quad (12)$$

where E_t is the incremental Young's modulus of the artery. Therefore, by taking the incremental axial stress of equation (12) into equation (9), the incremental axial tension and bending moment can be obtained:

$$\begin{aligned} \tilde{N} &= N = \overline{\sigma}_z A \\ \Delta M &= \frac{E_t\pi^2 I}{L^2}(\tilde{C}-C)\cdot\sin\left(\frac{\pi z}{L}\right) \end{aligned} \quad (13)$$

where A is the cross sectional area $A = \pi[(a+t)^2 - a^2]$, $\overline{\sigma}_z$ is the average axial stress and

$$I = \int_A (r\cos\varphi)^2 dA \quad (14)$$

is the bending moment of inertia of the wall cross section with $I = \pi[(a+t)^4 - a^4]/4$ for the cylindrical vessels.

Combining Equations (13) and (7) and reorganizing yields

$$p = \frac{E_t \pi^2}{L^2}\left(\frac{I}{\pi a^2}\right) + \overline{\sigma}_z \frac{A}{(\pi a^2)} \tag{15}$$

Therefore, arteries buckle when the internal pressure reaches this critical pressure. When the wall is thin $I \approx \pi a^3 t$, and $A \approx 2\pi a t$, equation (15) becomes:

$$p_{cr} = \frac{E_t \pi^2}{(L/a)^2}\left(\frac{t}{a}\right) + 2\overline{\sigma}_z\left(\frac{t}{a}\right) \tag{16}$$

This equation is the same as the previous buckling equation (Han 2007), when the wall is linear elastic.

3 Results

Theoretical studies were performed to determine the effects of arterial wall dimensions, axial stress, and axial stretch ratio on the critical buckling pressure.

3.1 The effect of arterial radius and wall thickness

The effects of arterial wall dimensions on the critical pressure are reflected/characterized by two parameters: the slenderness ratio L/a and wall thickness to radius ratio t/a. The relationship between the critical pressure and the slenderness ratio L/a, and wall thickness to radius ratio t/a are illustrated in Figure 4. At given modulus and axial stress (or axial stretch ratio), the critical pressure increases with decreased (L/a) ratio or increased wall thickness to radius ratio (t/a). At fixed wall thickness and length, increasing the radius reduces critical pressure. However, for arteries with similar wall thickness to radius ratio, those arteries with larger radii would have a higher critical pressure. It is also seen that the thick-walled model and the thin-walled model give comparable predictions when the wall thickness to radius ratio is less than 0.2 (Figure 4 bottom). For porcine carotid arteries under physiological pressure, the ratio is 0.2 -0.3 and the thin-wall approximation gives an error of about 10-15%.

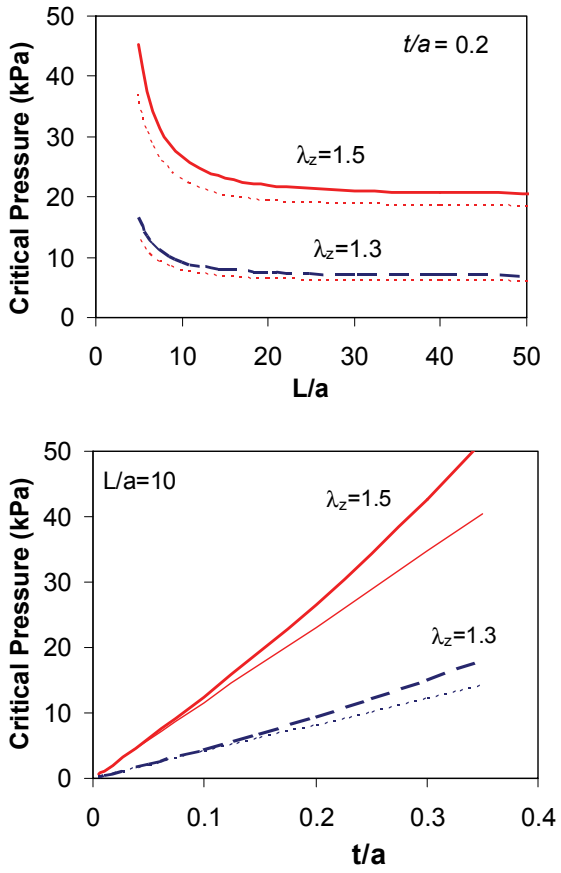

Figure 4: The critical pressure plotted against slenderness ratio L/a (Top) and wall thickness to radius ratio t/a (Bottom) at two given axial stretch ratios. The thin dot lines are the thin wall model approximations.

3.2 The relationship between the axial stress (stretch ratio) and critical pressure

Model equation (15) shows a linear relationship between the critical pressure and the axial stress (or the axial stretch ratio if the wall is linear elastic). However, the relationship is actually nonlinear for a given artery (even if the wall is linear elastic) if we consider the fact that the lumen radius actually changes with lumen pressure. To illustrate the nonlinear relationship between critical pressure and axial stress or axial stretch ra-

tio, we simulated the critical pressure in arteries with the Fung's exponential stress-strain relationship (Fung 1993):

$$\sigma_i = \beta(e^{\alpha(\lambda_i-1)}-1), \quad i=\theta,z,$$
$$\lambda_\theta = (a+\frac{t}{2})/(a_0+\frac{t_0}{2}), \quad \lambda_z = L/L_0 \tag{17}$$

Wherein α and β are material constants with values of 4.54 and 5.33 (kPa), respectively, and the wall was assumed isotropic based on our experimental data (Fierro et al. 2007; Han 2007). Our simulation showed that the critical pressure demonstrated a nonlinear increase with increasing axial stress and axial stretch ratio (Figure 5). The thin wall model under-estimated the critical pressure in the higher axial stress or axial stretch ratio range (Figure 5 Top and middle). Since the lumen radius increases with increasing pressure, ignoring the radius change and using a constant radius would overestimate the critical pressure especially in the higher axial stretch ratio range (Figure 5 bottom). Compared to a constant radius, the increase of lumen radius associated with pressure increase actually reduces the critical pressure. In general, increasing the axial tension or axial stretch ratio would increase the critical pressure and thus improve the stability of arteries, and vise versa.

4 Discussion

This study developed the buckling equation for arteries with a small initial curvature. The model results demonstrated that the buckling pressure changes dramatically with the axial tension or axial stretch ratio. These results significantly advance our knowledge of arterial buckling by considering thick-walled arteries with an initial curvature and material nonlinearity. The main conclusions are in general agreement with our previous results.

4.1 Model limitations and applications

While the model equations were derived for slightly curved arteries, the equations are applicable to straight arteries by letting $C = 0$ in the equations. In this case, the lateral load $q(z)$, bending moment M, and lateral reaction force Q be-

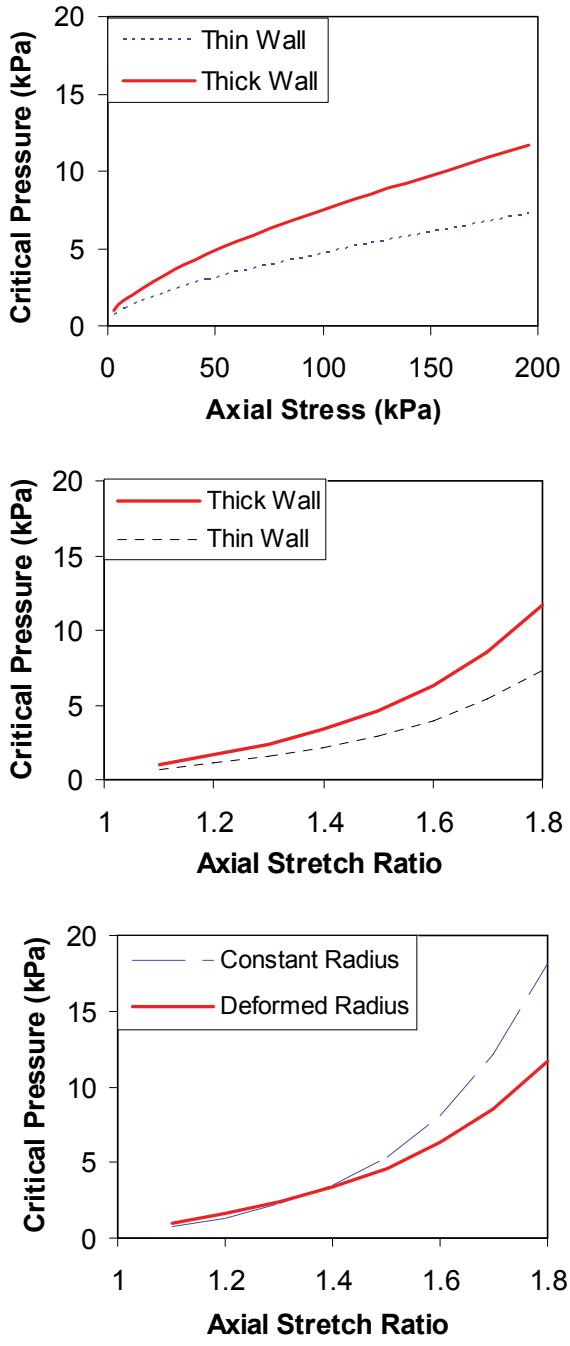

Figure 5: The nonlinear relationships between the critical pressure and the axial stress (Top) and axial stretch ratio (Middle & Bottom) with the material nonlinearity and changes in lumen radius taking into account (see text for details). It is seen that the critical pressure increases nonlinearly with axial stress and axial stretch ratio.

fore buckling given in equations (3) to (5) become zero. Thus, the lateral loads only occur when the arteries buckle. Nevertheless, buckling equations (15) to (16) hold true for both straight and slightly curved arteries. In addition, while the model equations were derived for simple-supported arteries, it can be generalized into other end restraints by using the "equivalent length" similar to the Euler column buckling (Gere 2004). Thus, the buckling equations can be applied to arteries with various end restrictions.

The limitations of the proposed model include the isotropic and homogeneous-wall assumptions. Arterial walls demonstrate a layered structure with different mechanical properties for the intima-media and adventitia layers (Fung 1993). The effect of this layered structure needs to be investigated in future studies. In this study, we examined only the incremental deformation at the initiation of bent buckling, which was treated as a small deformation with an incremental modulus at the stress level produced by the critical pressure. Our simulations were based on the isotropic assumption using Fung's uni-axial exponential stress-strain equation. Arteries generally have large deformations with a 3-D nonlinear stress-strain relationship. Further analysis is needed to include the 3-D and large nonlinear deformation nature of the arterial wall.

Another limitation of the current model is that the effect of contiguous tissue tethering was ignored in the current model. The effect of tissue tethering needs to be investigated in future studies. It is worth noting that the lumen pressure used in the model should be treated as the transmural pressure.

4.2 Clinical relevance

Arterial buckling can lead to arterial tortuosity in the long-term. Buckling alters the wall stress distribution in the arteries and thus affects cellular function and causes uneven matrix remodeling (Stein et al. 1994; Vorp et al. 1999) which, in the long run, may lead to abnormalities in the arteries. In fact, tortuosity has been observed in rabbit carotid arteries after the axial tension was reduced below the physiological level for a few weeks (Jackson et al. 2005).

The stability of living tissues and organs is an important issue in maintaining their normal function. The current model and critical load equation will be very useful in determining the critical level of the axial strain needed in arteries and veins in reconstructive vascular surgeries and vascular grafting in order to prevent tortuosity or kinking. In addition, the buckling equation can be useful for veins and other tubular biological structures, organs, and organelles.

Acknowledgement: This work was supported by a CAREER award from the National Science Foundation through grant #0644646, and was also partially supported by grant #0602834 from the National Science Foundation. The author thanks Ms. Patricia Navarro for proofreading the manuscript.

References

1. Dawson, D. L., J. C. Hellinger, T. T. Terramani, S. Najibi, L. G. Martin and A. B. Lumsden (2002). "Iliac artery kinking with endovascular therapies: technical considerations." *J Vasc Interv Radiol* **13**(7): 729-33.

2. Del Corso, L., D. Moruzzo, B. Conte, M. Agelli, A. M. Romanelli, F. Pastine, M. Protti, F. Pentimone and G. Baggiani (1998). "Tortuosity, kinking, and coiling of the carotid artery: expression of atherosclerosis or aging?" *Angiology* **49**(5): 361-71.

3. Fierro, C. A., K. Johnson and H. C. Han (2007). *The critical buckling pressure of arteries* ASME 2007 Summer Bioengineering Conference (SBC2007) Keystone, Colorado.

4. Fung, Y. C. (1993). *Biomechanics: Mechanical Properties of Living Tissues*. New YorK, Springer Verlag.

5. Gere, J. M. (2004). *Mechanics of Materials*, Thomson.

6. Han, H. C. (2007). "A biomechanical model of artery buckling." *J Biomech* **40**(16): 3672-8.

7. Han, H. C. and Y. C. Fung (1995). "Longitudinal strain of canine and porcine aortas." *J Biomech* **28**(5): 637-41.

8. Humphrey, J. D. (2002). *Cardiovascular Solid Mechanics: Cells, Tissues, and Organs*. New York, Springer.

9. Jackson, Z. S., D. Dajnowiec, A. I. Gotlieb and B. L. Langille (2005). "Partial off-loading of longitudinal tension induces arterial tortuosity." *Arterioscler Thromb Vasc Biol* **25**(5): 957-62.

10. Metz, H., R. M. Murray-Leslie, R. G. Bannister, J. W. Bull and J. Marshall (1961). "Kinking of the internal carotid artery." *Lancet* **1**: 424-6.

11. Nichols, W. W. and M. F. O'Rourke (1998). *McDonald's Blood Flow in Arteries: Theoretical, Experimental, and Clinical Principles. 4th Edition. Chapter 16.* London, Arnold Publisher.

12. Pancera, P., M. Ribul, B. Presciuttini and A. Lechi (2000). "Prevalence of carotid artery kinking in 590 consecutive subjects evaluated by Echocolordoppler. Is there a correlation with arterial hypertension?" *J Intern Med* **248**(1): 7-12.

13. Stein, P. D., M. S. Hamid, K. Shivkumar, T. P. Davis, F. Khaja and J. W. Henry (1994). "Effects of cyclic flexion of coronary arteries on progression of atherosclerosis." *Am J Cardiol* **73**(7): 431-7.

14. Thore, C. R., J. A. Anstrom, D. M. Moody, V. R. Challa, M. C. Marion and W. R. Brown (2007). "Morphometric analysis of arteriolar tortuosity in human cerebral white matter of preterm, young, and aged subjects." *J Neuropathol Exp Neurol* **66**(5): 337-45.

15. Vorp, D. A., D. G. Peters and M. W. Webster (1999). "Gene expression is altered in perfused arterial segments exposed to cyclic flexure ex vivo." *Ann Biomed Eng* **27**(3): 366-71.

16. Weibel, J. and W. S. Fields (1965). "Tortuosity, Coiling, and Kinking of the Internal Carotid Artery. I. Etiology and Radiographic Anatomy." *Neurology* **15**: 7-18.

17. Weibel, J. and W. S. Fields (1965). "Tortuosity, Coiling, and Kinking of the Internal Carotid Artery. II. Relationship of Morphological Variation to Cerebrovascular Insufficiency." *Neurology* **15**: 462-8.